JOURNAL OF SYNCHROTRON RADIATION

ISSN 1600-5775

The first infrared beamline at the Middle East SESAME synchrotron facility

Gihan Kamel,[a]*‡ Stephane Lefrancois,[b] Thierry Moreno,[b] Mohammad Al-Najdawi,[a] Yazeed Momani,[a] Anas Abbadi,[a] Giorgio Paolucci[a,c] and Paul Dumas[b]

[a]SESAME Light Source (Synchrotron Light for Experimental Science and Applications in the Middle East), Allan, As-salt, Jordan, [b]Synchrotron SOLEIL, L'Orme des Merisiers, F-91192 Gif Sur Yvette, France, and [c]Elettra Sincrotrone SCpA, SS 14 Km 163,5 in AREA Science Park, IT-34149 Basovizza, Trieste, Italy. *Correspondence e-mail: gihan.kamel@sesame.org.jo

Received 23 June 2021
Accepted 22 August 2021

Edited by I. Lindau, SLAC/Stanford University, USA

‡ On leave from Department of Physics, Faculty of Science, Helwan University, Cairo, Egypt.

Keywords: SESAME synchrotron; infrared beamline; design; construction; FTIR microspectroscopy.

SESAME (Synchrotron-light for Experimental Science and Applications in the Middle East) is the only synchrotron light facility in the Middle East and neighboring regions, officially opened in 2017. Among the identification and construction of the first operational beamlines, infrared spectromicroscopy was selected as one of the two beamlines to be opened to the general users' program (the so-called Day-1 beamlines). Being one of the most demanded techniques by various scientific communities in the Middle East, the beamline has been designed and implemented in the framework of a collaboration agreement with the French synchrotron facility, SOLEIL. The design, construction and initial performances of the IR beamline (D02-IR), nowadays operational, are reported.

1. Introduction

SESAME aims at promoting advanced research and technology within its Members and neighboring regions. Current SESAME Members are Cyprus, Egypt, Iran, Israel, Jordan, Pakistan, Palestine and Turkey; current Observers are Brazil, Canada, China, the European Union, France, Germany, Greece, Italy, Japan, Kuwait, Portugal, the Russian Federation, Spain, Sweden, Switzerland, United Kingdom and United States of America. Infrared spectroscopy is a nondestructive multidisciplinary vibrational technique of strong interest at synchrotron facilities that has demonstrated over the years its marked and complementary advantages compared with infrared laboratory-based sources. With equivalent success among the synchrotron radiation facilities around the world, infrared synchrotron spectroscopy and microscopy prove distinct competence in different fields such as physics, chemistry, biology, geology, biomedical arenas, agricultural, environment and materials science, cultural heritage and bio-archeology among others. In the case of SESAME, the infrared beamline is the first completely designed and built beamline, and has been selected together with the XAFS/XRF (X-ray absorption fine structure/X-ray fluorescence) beamline for the initial operational phase. The design of the beamline (optical setup, mechanical and vacuum components) has been adapted to fit into the limited space between the storage ring in construction and the exit tunnel wall, as well as the available experimental floor space. The optical setup has been optimized by simulation using two main software packages, *SRW* (Chubar & Elleaume, 1998) and *SpotX* (Moreno & Idir, 2001), while the details of the mirror mountings and the location of all instruments on the experi-

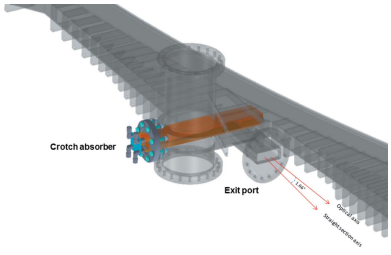

Table 1
SESAME machine parameters.

Parameter	Description	Value
E	Electron energy	2.5 GeV
B	Magnetic field	1.4554 T
R	Bending radius	5.726 m
I	Electron current	400 mA
L	Straight section length	4.4 m

mental floor have been designed using *SolidWorks* (Dassault System, https://www.solidworks.com). The aim of this paper is to describe the optical layout of the beamline and to provide an evaluation of its actual brilliance, which is a measure of the performance of the synchrotron infrared endstation.

2. Infrared extraction scheme

SESAME is a 2.5 GeV third-generation electron storage ring optimized for producing high-brightness synchrotron radiation (Varnassari, 2005). The main source parameters are listed in Table 1. A 20 MeV microtron injects the electrons into an 800 MeV booster synchrotron, with 1 Hz repetition rate. The 800 MeV beam is transported through the transfer line to the main storage ring and, after accumulation, is accelerated to 2.5 GeV.

The electron current has been ramped up progressively by time, and presently the operating electron current is 300 mA. The ultimate goal of the facility is to reach an electron current of 400 mA. The beamline design has been guided by the objective of providing an optimized photon flux in the mid-IR range while exhibiting significantly enhanced performance in terms of brightness, compared with a conventional source, in both the far-IR and mid-IR regions. Due to the larger angles of emission of the infrared photons, the dipole chamber had to be modified. The restrictions of the actual dipole chamber modifications at the SESAME main storage ring (Varnassari, 2005) have imposed limitations on the optimum collection geometry of the infrared emission. Figure 1 shows the modified dipole chamber, whose extraction geometry limits the opening angles to 39 mrad horizontally and 15 mrad vertically. Since both edge radiation and constant field emission are collected, the first collection mirror is positioned such that the optical axis for the beamline is located at 1.66° inward of the straight section axis.

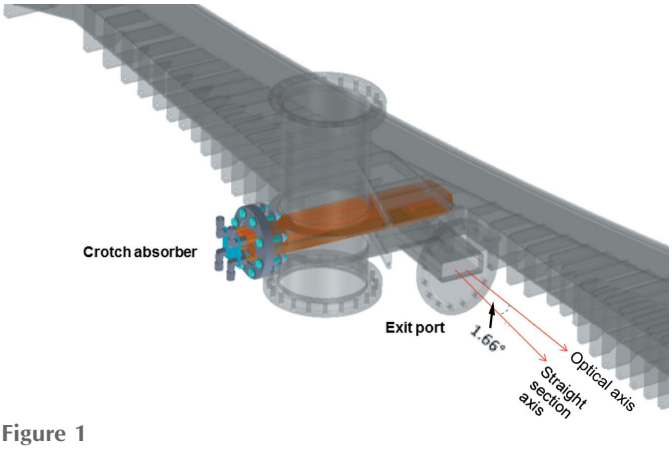

Figure 1
The beamline modified dipole chamber including the crotch absorber, which is a heat mask component to protect the dipole chamber walls from absorbing the extra large amount of synchrotron radiation in the storage ring.

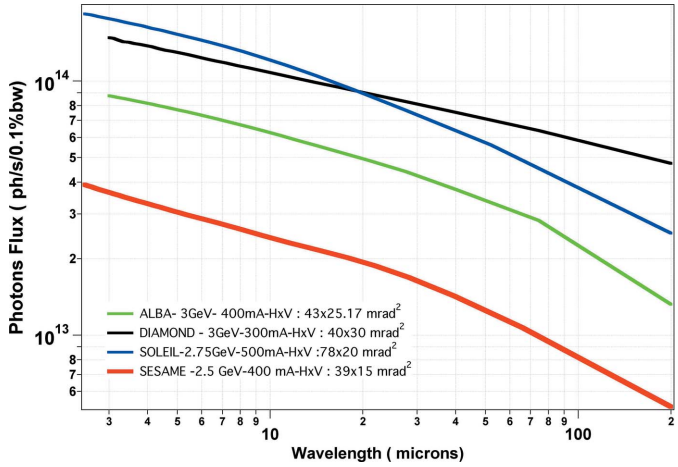

Figure 2
Photon flux comparison between SESAME and four recently operational beamlines collecting the edge emission and constant field emission in Spain (ALBA), France (SOLEIL) and UK (Diamond). The differences in the emitted flux rely upon different operating electron energy and current, and different collected solid angles. Calculations have been carried out using *SRW*.

The IR beamline is designed in such a way that it will optimally utilize the infrared synchrotron radiation from two main emission sources; edge radiation and constant field of the bending magnet (Dumas *et al.*, 2020). As such, the infrared source of the beamline can be considered as an incoherent superposition of the two sources. Accounting for the modifications of the dipole chamber, and considering the ultimate operating electron current at SESAME (400 mA), the infrared photon flux has been calculated using *SRW*, and compared with three beamlines from other synchrotron sources (Fig. 2). This figure shows that the infrared flux at SESAME is less than that at the three other beamlines. This is explained by the limited vertical and horizontal angles of the modified dipole chamber. Each facility is facing constraints regarding such modifications depending upon the position and size of the subsequent magnetic devices, and it is the case with SESAME.

Beam extraction was accomplished using a combination of mirrors, collecting the infrared radiation and focusing it through a 0.5° wedged CVD (chemical vapour deposited) diamond window. This window separates the storage ring ultra-high-vacuum environment from the endstation low-vacuum environment.

3. Simulation and optical setup

3.1. Initial wavefronts

Two software packages have been used to simulate the wavefronts at various wavelengths, and their propagation

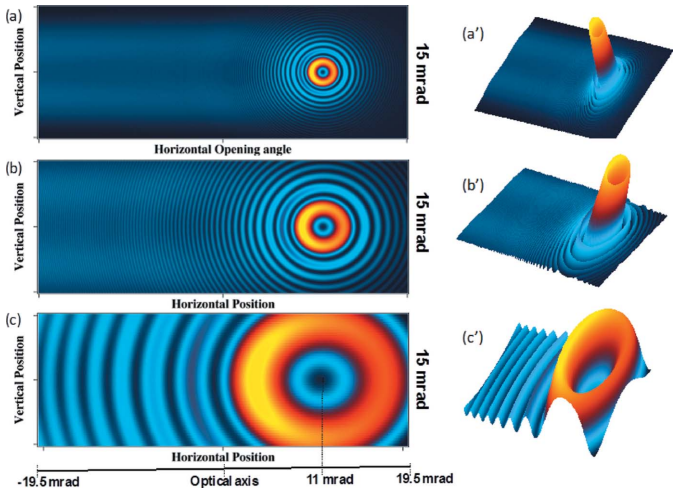

Figure 3
2D and 3D images, respectively, of the initial wavefronts, at 2145.5 mm from the source and at 3 µm (*a* and *a*′), 10 µm (*b* and *b*′) and 100 µm (*c* and *c*′).

to the experimental station: *SRW* (Chubar, 2001, 2006) and *SpotX* (Moreno & Idir, 2001). *SRW* provides a collection of computational tools for various simulations of the processes of emission in bending magnets and insertion devices, as well as the propagation of the radiation using Fourier optics propagation, while *SpotX* is a ray-tracing program. Expected performances in terms of flux and spatial distribution of the photons have been calculated and compared. Considering the various above-mentioned constraints, the optimum position of the first extraction mirror is at 2145.5 mm from the source. The infrared wavefronts, calculated using *SRW*, for three prototypical wavelengths (3 µm and 10 µm for the mid-IR, and 100 µm for the far-IR) are displayed in Fig. 3.

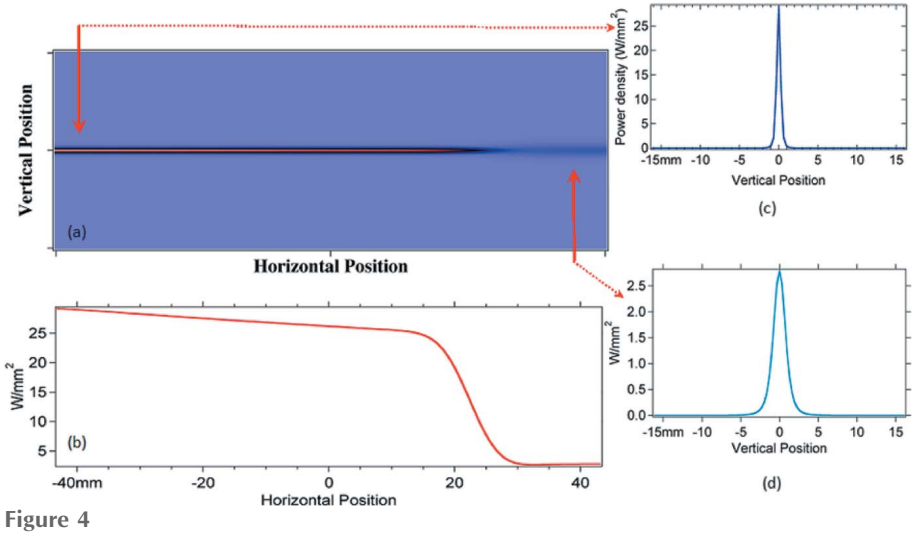

Figure 4
(*a*) Power density on the first plane mirror, located at 2145.5 mm from the source. (*b*) Power distribution along the horizontal direction: Note the rapid change in power heat load from edge radiation to constant field emission. (*c*) Vertical cut of the constant field emission, at the location indicated by the left-hand arrow. (*d*) Vertical cut inside the edge radiation emission (right arrow).

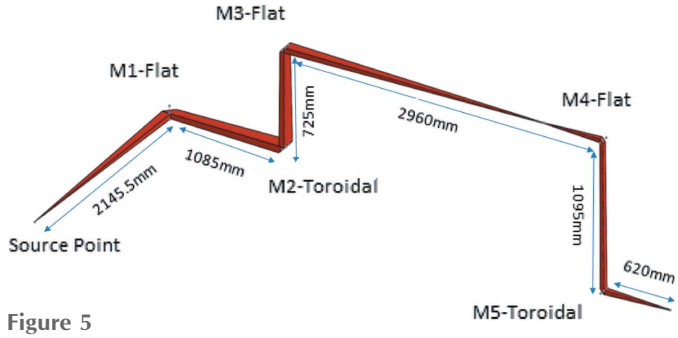

Figure 5
Beamline optical pathway.

3.2. Heat load

Coping with heat load at the first extracting mirrors is a problem of serious concern, and must be addressed accurately. Severe damage of the first mirror due to excessive heat load has occurred at some infrared beamlines. Figure 4 reports the power density calculated at the first mirror position, using *SRW*.

The heat load reaches its maximum at the extreme end of the constant field emission (close to 30 W mm^{-2}). As for several operational beamlines, we opted for a central slot of 3 mm in the first mirror, to leave the 'hard' beam reaching an absorber located behind the mirror.

3.3. Optical setup

The optical setup has accounted for the limited space between the beam extraction from the dipole chamber and the nearby tunnel wall, for the need to remove radioprotection issues by raising the exit hole through the tunnel to the experimental station above the orbit plane, and the close location of the instrument in the experimental floor from the tunnel wall. Figure 5 shows a sketch of the optical pathway from the source to the experimental hutch. The optics parameters and distances are reported in Table 2.

After exiting through the KBr window, the beam is directed toward an optical coupling box, for reshaping the beam, and collimates it to a size compatible for the entrance of the external port of the FTIR spectrometer. Two sets of cylindrical mirrors (M6 and M7) were used to collimate the beam with a squared shape of about 30 mm size.

Using *SpotX* and *SRW*, we confirm the results at the first focal point (right after the CVD diamond window) and at the second focal point, after the KBr window and before collimating the beam for entering the spectrometer (Fig. 6).

The two software packages give an almost equivalent image size – the

Table 2
Optical setup, nature, parameters and distances.

Component	Distance from source (mm)	Position from previous optical element (mm)	Mirror type
M1 (slot 3 mm)	2145.5	2145.5	Plane Θ = 45°, sideward
M2	3232	1086.5	Toroidal Θ = 45°, upward, tangential radius = 4.5011 m, sagittal radius = 2.2505 m
M3	3957	727	Plane Θ = 45°, downward
Focal plane	6367	2410	Diameter = 20 mm, CVD 500 µm, wedge 0.5°
M4	6917	550	Plane Θ = 45°, downward
M5	7977	1060	Toroidal Θ = 45°, upward, tangential radius = 1.744 m, sagittal radius = 0.872 m
Second focus	8977	1000	KBr window
M6	9177	200	Horizontal collimation, sagittal cylinder, radius = 282.84 mm, upward
M7	9327	150	Vertical collimation, tangential cylinder, radius = 989.94 mm, downward

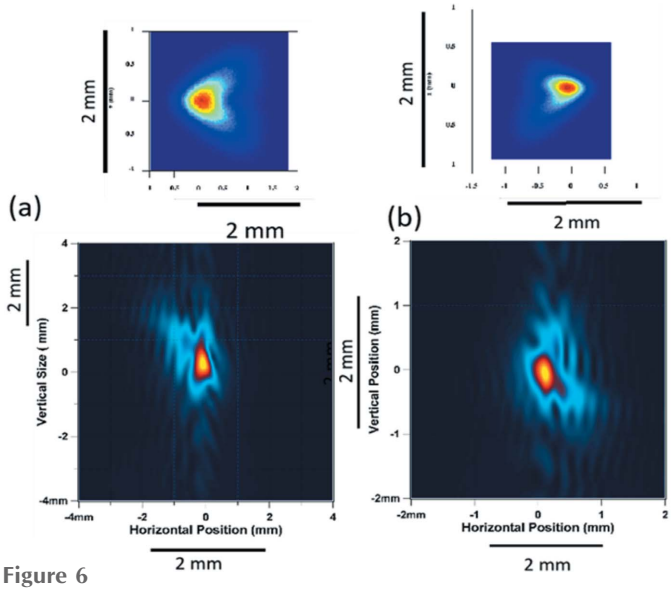

Figure 6
Simulation of the beam, for a wavelength of 10 µm, at the two intermediate focused images of the source: (*a*) at the first focus and (*b*) at the second focus. The main images have been calculated using *SRW* (bottom), while the top images have been calculated using *SpotX*. *SRW* and *SpotX* simulations are on the same scale and provide consistent results despite the nature of the simulation (Fourier optics propagation versus ray tracing).

difference in shape originates from the fact that *SRW* is the most appropriate software in the case of SESAME for the propagation of edge radiation, since the propagation of the wavefront accounts for the near-field effect, which is hardly accounted for with ray-tracing software.

4. Beamline components

The beamline inside the tunnel consists of three main cells: dipole chamber, M1 extraction chamber and (M2–M3) focusing chamber. Au-coated aluminium (20 nm thickness) for the first extracting mirror M1 and bare aluminium for the remaining mirrors were chosen as materials for the optical elements. A sketch of the whole beamline is shown in Fig. 7.

4.1. From source to the first focus point

As shown in Fig. 8, the beamline components from the source to the first focus point start with the first optical component M1 (3 mm-slotted plane mirror) that is placed at a distance of 2145.5 mm from the source point. The two main functions of this mirror are to filter out the hard X-rays beam (radiation above 20 eV) and to deflect the infrared at 90° in the horizontal plane. A combination of a toroidal (M2) and a plane (M3) mirror focuses the IR radiation, after passing through the tunnel wall, onto a wedged CVD (0.5°, 500 µm average thickness) diamond window of 20 mm clear aperture. Strict safety and control procedures are applied to M1 to avoid its damage during the beam injection. The beam is redirected outside the tunnel wall with the first focus at a distance of 6367 mm from the source.

4.2. IR extraction mirror: M1

The first mirror M1 is a plane mirror with a slot of 3 mm vertical opening. The size of the slot has been determined by calculating the heat power distribution at the center of the mirror using *SRW*, for a beam current of 400 mA (see Fig. 4). The calculation shows that the mirror will have to subtend 32 W mm^{-2} at the most, and can be damaged without a very efficient cooling system, or a mask preventing the white beam

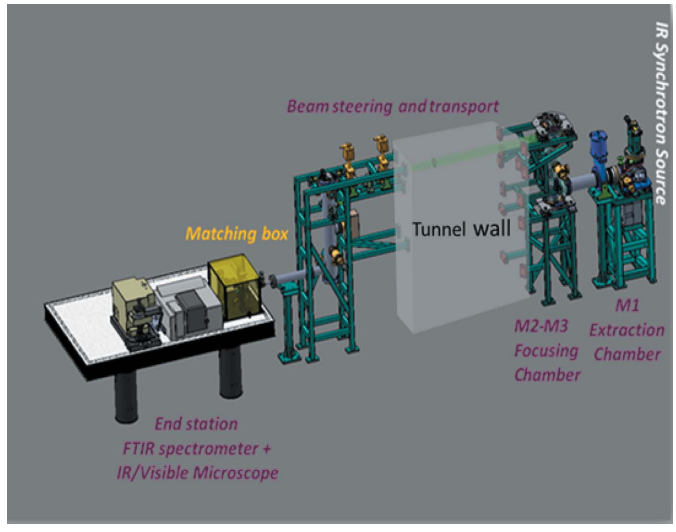

Figure 7
Sketch of the beamline components from the extraction chamber to the instrumental endstation.

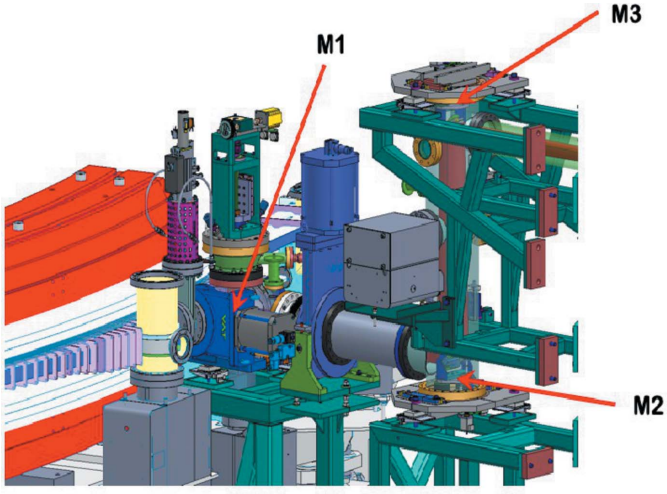

Figure 8
Beamline components inside the storage ring: first extraction mirror M1 and its chamber, M2 (toroidal) and M3 (plane) flange mirrors in their UHV chamber.

from reaching the mirror. The mirror is mounted at the end of an arm, which can be moved by more than 25 mm, using step motors and precise translational motion [Fig. 9(*a*)]. This allows a precise repositioning of M1 after each retraction. The temperature of the mirror is surveyed by ten thermocouples, whose locations are indicated in Fig. 9(*b*). An absorber positioned downstream of M1 dissipates the low-divergence high-energy part of the radiation passing through the M1 slot.

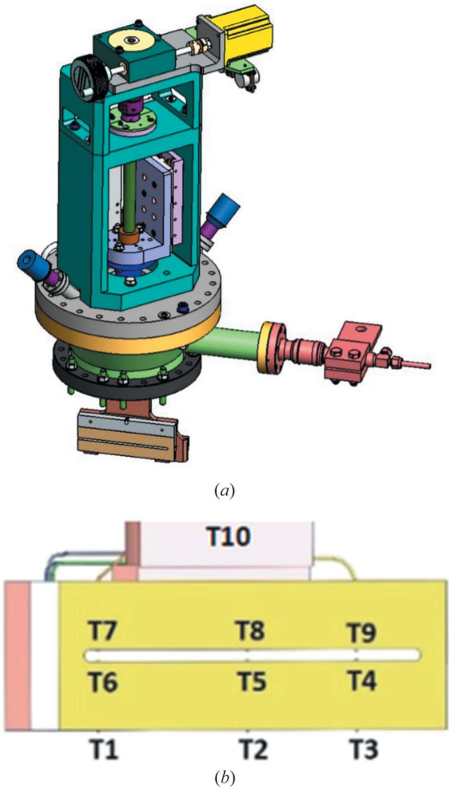

Figure 9
(*a*) IR extraction mirror, M1. (*b*) M1 surveying thermocouples.

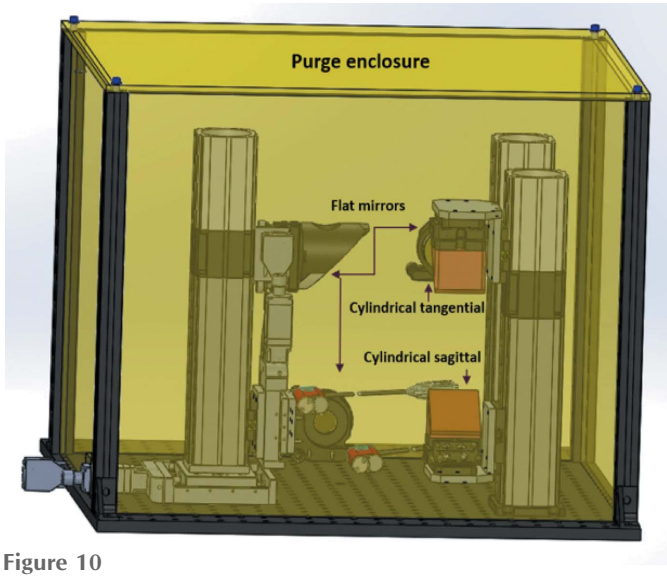

Figure 10
Optical coupling box.

4.3. From first focus point to the entrance of the spectrometer

After being focused at the exit of the tunnel wall, inside the experimental hutch, the beam then proceeds in high vacuum inside the experimental hall where it is collimated by the optical coupling box, two cylindrical mirrors, and sent towards the experimental endstation. The propagation of the beam continues to the entrance of the FTIR spectrometer. A pair of plane and toroidal mirrors have been set inside a high-vacuum vessel, in order to produce a second focus point at the level of the spectrometer entrance. A KBr window, positioned at the second focus, allows to separate the vacuum to the purged atmosphere of the beam reshaping enclosure, that we call the coupling box (Fig. 10), and the spectrometer to which the microscope is coupled. The optical coupling box aims at producing a collimated beam of approximately 30 mm × 30 mm, with several degrees of freedom, to allow a fine coupling with the interferometer through the external port of the spectrometer.

5. Vacuum system

The ultra-high-vacuum section of the beamline stands between the exit port of the dipole chamber and the wedged CVD diamond window located beyond or after the tunnel wall. The vacuum components layout is displayed in Fig. 11

A differential pumping system is implemented around the CVD diamond window that is used to separate the UHV inside the tunnel from an enclosed high-vacuum environment in the remainder of the beamline. The front-end chamber is composed of a photon shutter which is followed by a gate valve connected to the dipole chamber. The extraction mirror, M1, deviates the beam horizontally toward a second gate valve for a complete vacuum isolation of this front-end chamber in case of M1 damage and replacement. The front-end chamber is also equipped with an independent ion pump (150 l s^{-1}), a

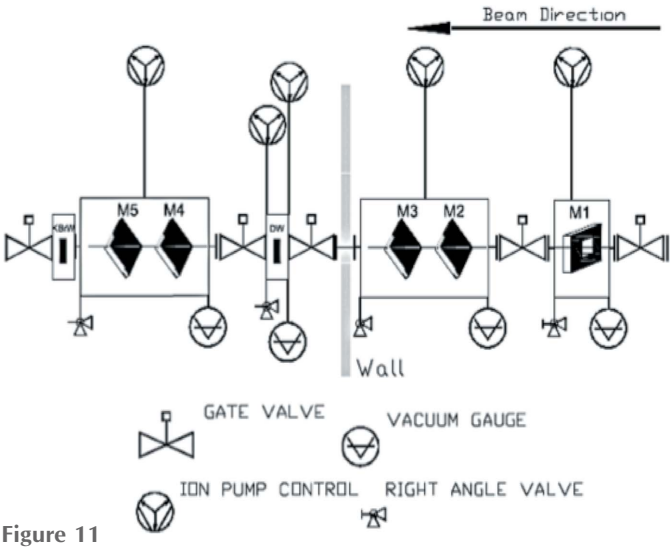

Figure 11
Beamline vacuum components layout.

gate valve for external pumping, and a gauge for pressure reading. The M1 holding mechanism and its associated manipulator has been the subject of careful consideration, taking into account previous experiences gained at other third-generation synchrotron radiation infrared (SRIR) beamlines. In order to avoid a fast valve shutter in the case of CVD window failure, two gate valves are placed upstream and downstream of the window, and high vacuum is kept permanent on both sides.

6. Control system

The *Experimental Physics and Industrial Control System* (*EPICS*) software has been utilized for the control system of SESAME's accelerator and beamlines. The beamline has its own control system and its own network (Fig. 12). Access to the Machine Control System network is allowed through a gateway in order to obtain parameters like machine current, energy, *etc*. Vacuum pumps and gauge controllers are controllable either via serial protocols or ethernet. The equipment protection system (EPS) in SESAME beamlines is designed to protect the hardware components of the beamline from any hazard or fault that could result from excessive heat, low flow of cooling water, and high gas pressure in the vacuum vessels, for instance in case of failures. This system has been implemented through a programmable logic controller (PLC).

7. Experimental endstation

Currently, one endstation is fed by beamline optics collecting both the bending and the edge synchrotron radiation. In a later stage, the beamline can be easily split into two branches, of equivalent path lengths and performances. The installation of a remote-controlled optical coupling box was envisaged (Fig. 10), like in other SRIR lines exploiting edge and constant field IR emission (ESRF, SOLEIL, Australian Synchrotron and Diamond) to match the interferometer optics with proper beam size and divergence.

The endstation (see Fig. 13) includes an 8700 Thermo Scientific FTIR spectrometer. The spectrometer is coupled to a Thermo Scientific Nicolet Continuum IR-microscope allowing spectro-microscopic chemical imaging studies, with differential interference contrast (DIC) and fluorescence microscopy capabilities (Kamel *et al.*, 2017).

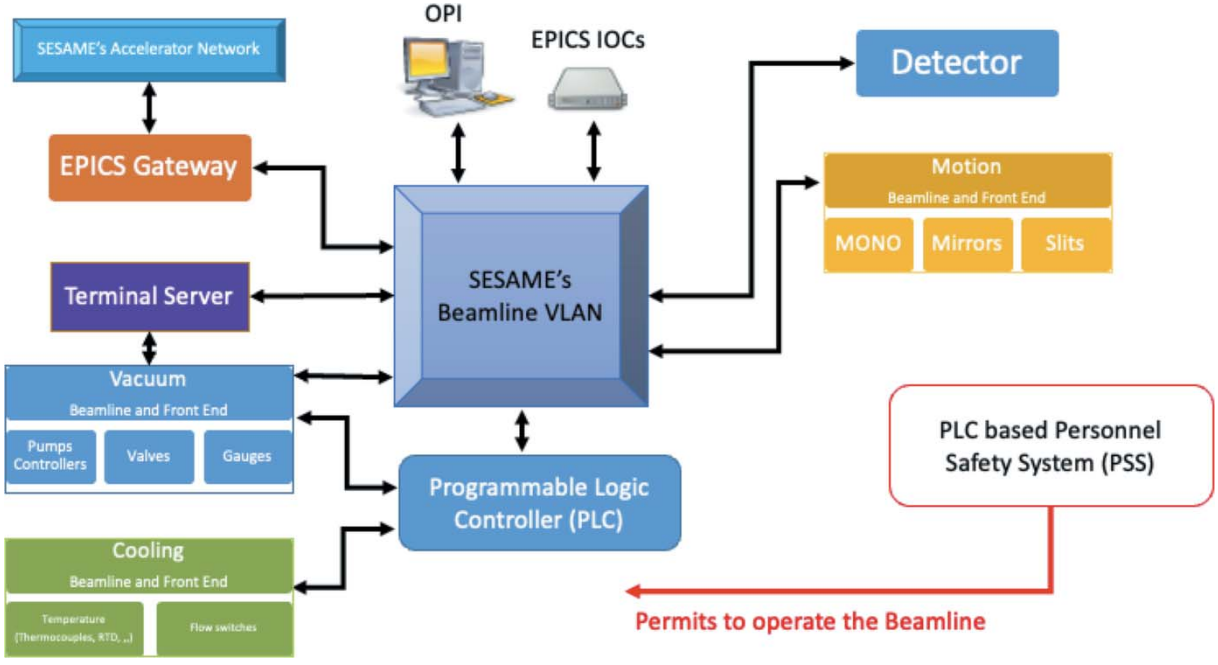

Figure 12
Beamline control system.

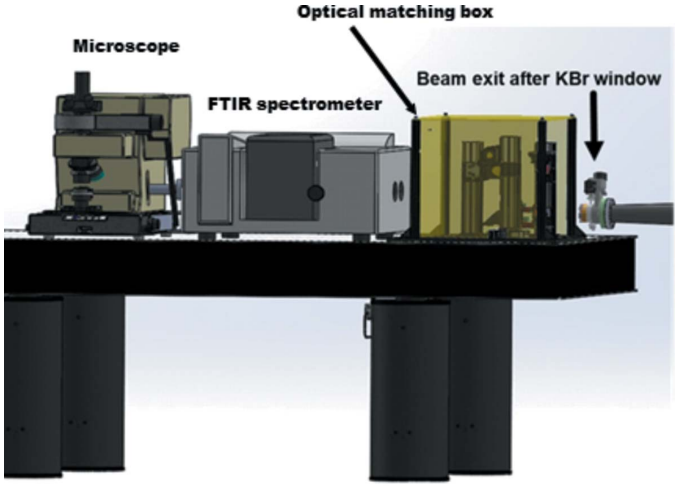

Figure 13
Beamline endstation.

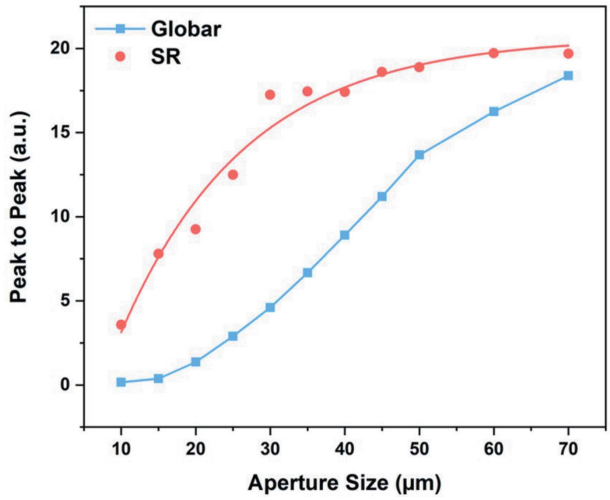

Figure 15
Peak-to-peak interferogram values (transmission mode, ×32 objective) of the synchrotron IR source (at 200 mA) versus the Globar source at different aperture sizes.

8. Performance

The synchrotron source exhibits a marked advantage in terms of brightness compared with a thermal source (Globar). Figure 14 shows the infrared signal obtained through a 10 μm × 10 μm aperture, with both sources. There is an increase of the signal through this aperture size of about a factor of 20, with a 200 mA electron current.

The spectrometer and the microscope are both purged with compressed air, while the sample's surrounding is exhibiting an atmospheric environment. Accordingly, absorption peaks due to the H_2O at 1600 cm^{-1} and 3800 cm^{-1} and the peaks due to the CO_2 at 2350 cm^{-1} are observed. There are three relatively strong absorption peaks observed at 2030 cm^{-1}, 2170 cm^{-1} and 2520 cm^{-1} with the synchrotron radiation spectrum, originating from absorption by the CVD diamond window. The ratio of the infrared signal with the various aperture sizes is one of the hallmarks of the beamline performances. Figure 15 shows the intensity variation for a squared aperture of 10 to 70 μm side, between the synchrotron infrared source and the Globar.

A gain is observed at almost all aperture sizes. Fig. 16 shows the intensity behavior, in reflection mode, for the two available Schwarzschild objectives at the beamline [×32, numerical aperture (NA) 0.68; ×15, NA = 0.5].

Despite the gain in intensity when the aperture closes, one of the characteristics of the beamline performance is the signal stability over time. Several noise sources can induce a spectral noise which is detrimental to the spectral quality. We performed a so-called stability test by recording two successive spectra at 4 cm^{-1} spectral resolution and 100 scans, with an aperture of 20 μm × 20 μm. The results, displayed in Fig. 17, clearly show the noise advantage provided by the beamline and for an aperture below 20 μm.

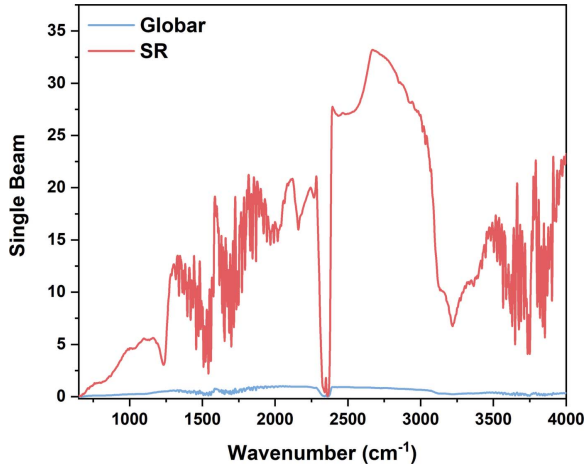

Figure 14
Single beam transmitted using the IR synchrotron radiation source (at 200 mA) and the Globar source with an aperture of 10 μm × 10 μm (265 co-added scans, resolution 8 cm^{-1}).

9. Summary

An infrared beamline is operational at SESAME, the first Middle East Synchrotron Facility. Selected among the two most demanded Day-1 beamlines by the users' community, the beamline has successfully achieved its goal in providing performances at the international level. The beamline exploits the emission of two sources: edge radiation and constant field with a 39 mrad (H) × 15 mrad (V) opening angle. The brightness advantage and the superior spectral quality obtained at small apertures illustrate the capabilities of the beamline. Since its opening to user programs, the beamline has welcomed 35 users from eight countries across the Middle East and Europe. The scientific program is diverse with strong emphasis on biology and cultural heritage. The photon flux is compatible for future beamline splitting with another spectrometer to satisfy the growing number of beam time requests.

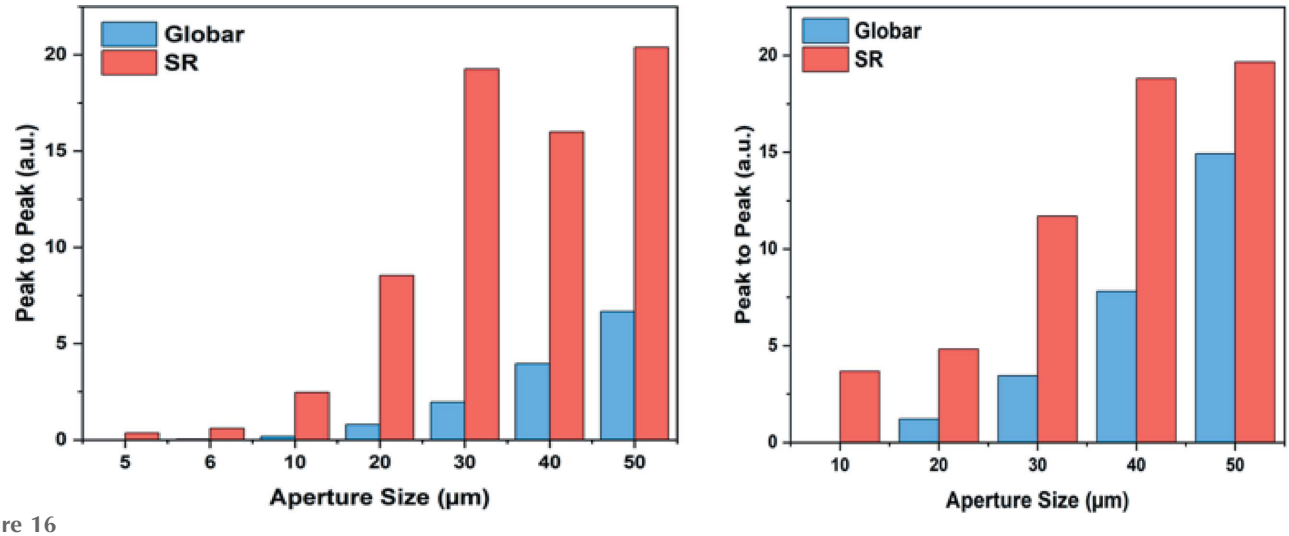

Figure 16
Reflection mode peak-to-peak interferogram values for both the synchrotron IR source (at 200 mA) and the Globar source at different aperture sizes for the 15× (top) and 32× (bottom) objectives.

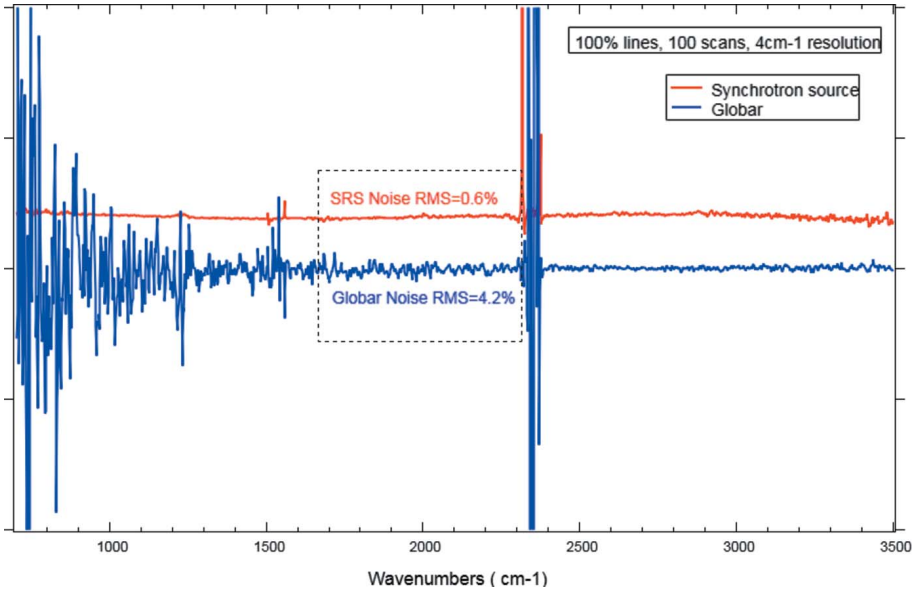

Figure 17
100% lines of SRIR and Globar sources through a 20 μm × 20 μm aperture (100 co-added scans at resolution 4 cm^{-1}) demonstrating their signal-to-noise comparison. The SRS 100% line has been offset for clarity.

Acknowledgements

The authors would like to thank all the people of both facilities SESAME and SOLEIL, involved with different expertise in fulfilling the mission of the beamline design, construction and successful operation. In particular, Adel Amro, Basil Aljamal, Abdallah Ahmed, Mahmoud Irsheid, Osama Nour, Sa'ed Budair, Farouq Al-Omari, Messaoud Harfouche, Mahmoud Abdellatief, Mustafa Al-zoubi, Salman Matalgah, Mohammad Al-Qtaishat, Tha'er Abu-Hanieh, Ismail Al-zoubi, Tamer Al-zoubi, Qusai Al-zoubi, Mohammad Khalaylah, Erhard Huttel, Riccardo Bartolini, Maher Attal, and Adli Hamad; as well as SESAME and SOLEIL Administrative Sectors.

References

Chubar, O. (2001). *Proc. SPIE*, **4143**, 48–59.
Chubar, O. (2006). *Infrared Phys. Technol.* **49**, 96–103.
Chubar, O. & Elleaume, P. (1998). *Proceedings of the Sixth European Particle Accelerator Conference (EPAC'98)*, Stockholm, Sweden, 22–26 June 1998, pp. 1117–1179.
Dumas, P., Martin, M. & Carr, G. (2020). *Synchrotron Light Sources and Free-Electron Lasers*, edited by E. Jaeschke, S. Khan, J. Schneider & J. Hastings, pp. 2059–2113. Springer.
Kamel, G., Lefrancois, S., Al-Najdawi, M., Abu-Hanieh, T., Saleh, I., Momani, Y. & Dumas, P. (2017). *Synchrotron Radiat. News*, **30**(4), 8–10.
Moreno, T. & Idir, M. (2001). *J. Phys. IV*, **11**, PR2-527–PR2-531.
Varnassari, S. (2005). *Proceedings of the 7th Diagnostics and Instrumentation for Particle Accelerators Conference (DIPAC 2005)*, 6–8 June, 2005, Lyon, France.